

Djordje S. Čantrak

University of Belgrade, Faculty of Mechanical Engineering, Hydraulic Machinery and Energy Systems
Department, Belgrade
Serbia

**ADVANCED RESEARCH IN ENERGY SYSTEMS
- BILATERAL PROJECT KARLSRUHE-BELGRADE**

**Resources of Danubian Region:
the Possibility of Cooperation and Utilization**

Editors

Luka Č. Popović

Melita Vidaković

Djordje S. Kostić

Belgrade
Humboldt-Club Serbien
2013

ISBN 978-86-916771-1-4

Donau

Dunaj

Duna



Dunărea

Donau

Abstract. Study of the complex turbulent vortex structures belongs to the class of the most complex problems of energetic and turbulence and has, not only theoretical, but also practical significance. Phenomenon of the swirl flow field and flow in rotating systems is present in various engineering systems including turbomachines, cyclones, vortex separators, burners, combustions systems and etc. Turbulent swirl flow field behind the axial fan impeller has been studied here by use of the modern laser based measuring techniques, such as laser Doppler anemometry (LDA), stereo particle image velocimetry (SPIV) and high speed SPIV (HSS PIV).

Key words: Axial fan, turbulence, swirl flow, invariants, lasers, LDA, HSS PIV.

1. Introduction

Investigation of the turbulent structure of the three-dimensional, inhomogeneous and anisotropic swirl flow behind axial fan of specific geometry is presented in this paper. Swirl flow has been investigated by numerous authors, what is considered in references [1-16]. This paper underlines investigation of the turbulent swirl flow in pipe behind an axial fan. Here are presented some experimental results of the researchers included in the Bilateral project "Investigation of the turbulent structure behind the axial fan impellers by use of the HWA, LDA and PIV measuring techniques and CFD analysis" (lasted in period 2011-2012.). Project has been a good frame for this complex problem of theoretical and applied fluid mechanics. Project has been established between the Faculty of Mechanical Engineering University of Belgrade, departments of Fluid Mechanics and Hydraulic Machinery and Energy Systems and Faculty of Mechanical Engineering, Institute of Fluid Machinery, Karlsruhe Institute of Technology. Twelve researchers were officially involved in the Project, equally from both sides. Experiments and computations were conducted in both faculties.

Study of the complex turbulent vortex structures belongs to the class of the most complex problems of energetic and turbulence and has, not only theoretical, but also practical significance. Phenomenon of the swirl flow field and flow in rotating systems is present in various engineering systems including turbomachines, cyclones, vortex separators, burners, combustions systems and etc. Investigated vortex structures are closely related to the problems of noise and vibrations in thermotechnical installations and other energy plants. Flow and energy characteristics of the turbulent swirl flow field behind the axial fan impeller has been studied by use of the modern laser based measuring techniques such as Laser Doppler Anemometry (LDA) and High Speed Stereo Particle Image Velocimetry (HSSPIV).

Obtained results enable taking into consideration swirl effects, rotation and vortex structures in the computation and construction of the technical systems where the swirl flow exists.

2. Experimental test rigs and techniques

Two experimental test rigs have been accomplished in order to study turbulent swirl flow behind axial fan.

2.1. Experimental test rigs

Test rig presented in Fig. 1., 27.74D long, where $D=0.4$ m is the average inner pipe diameter, has been built at the Faculty of Mechanical Engineering University of Belgrade, Laboratory for Hydraulic machinery and energy systems in the seventies of the previous century.

Numerous experimental investigations have been performed on this test rig, of which one of the most important are [1,2,4]. This test rig has been upgraded to the level of sophisticated hot-wire anemometry

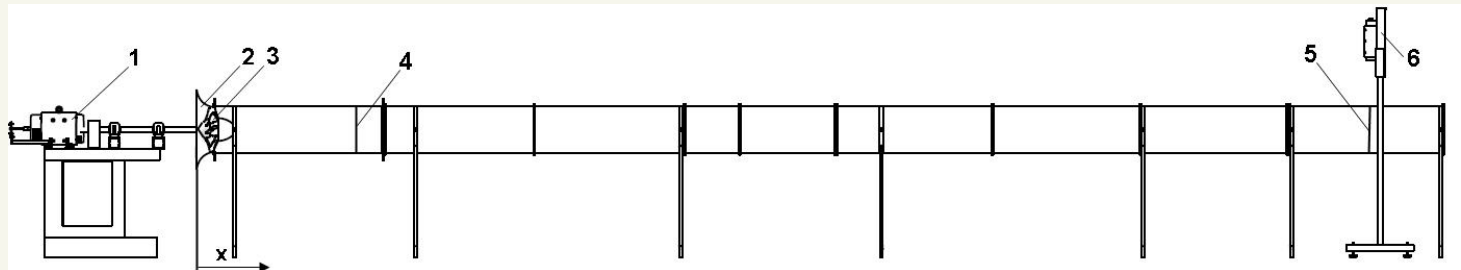


Figure 1. Experimental test rig: 1 -DC motor, 2-profiled free bell-mouth inlet, 3-axial fan, 4 and 5 LDA and SPIV measuring sections, 6-Nd:Yag laser.

measurements in [4], and afterwards for laser based measurements in [1]. An axial fan is positioned at the test rig inlet, i.e. in the first acrylic glass section, $3.75D$ long. This section is followed by the plastic non-transparent ducts, and one additional transparent section, $3.45D$ long at the end. The stereo particle image velocimetry (SPIV) and laser Doppler anemometry (LDA) measurements have been performed in two sections $x/D=3.35$ and $x/D=26.31$, of which the first one is denoted as "1" and the second one as "2". The coordinate x is measured from the test rig inlet (Fig. 1.), i.e. from the profiled free bell-mouth inlet.

The axial fan with variable impeller angle is designed by Protić[†]. It has nine blades and has been constructed after the law $rW=\text{const.}$, where W is a time-average circumferential velocity. The outer impeller diameter is $D_a=0.399$ m. The dimensionless hub ratio is $D_i/D_a=0.5$, where D_i is a hub diameter. The blade angle at impeller diameter for these experiments was adjusted to 30° .

The second test rig was built at the Faculty of Mechanical Engineering, Institute of Fluid Machinery, Karlsruhe Institute of Technology (Fig. 2.). The same swirl flow generator has been employed. Also, the same acrylic duct at the inlet, has been used.

Experimental test rig is, here, designed with an axial fan at the inlet in acrylic pipe, followed by the aluminum duct. Total length is app. $20D$, where $D=2R\approx 0.402\text{m}$ is inner diameter. This measurement

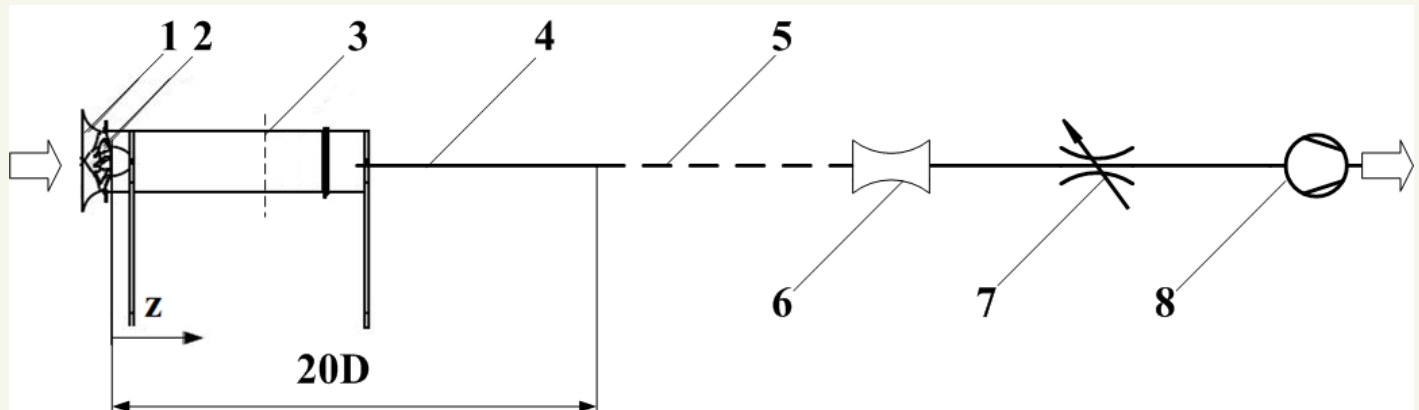


Figure 2. Experimental test rig for HSS PIV measurements: 1-free bell-mouth inlet, 2-axial fan, 3-measuring section ($x/D=2.1$) in acrylic pipe, 4-aluminium duct, 5-exhaust, flexible hose, 6-venturi flow rate meter, 7-choke and 8-booster fan.

section is connected to the exhaust hose which leads to the venturi flow meter, regulation valve and booster fan (Fig. 2.). Measurements have been performed behind the axial fan, in the pipe cross-section and horizontal meridian section with center in position $z=2.1D$ measured from the blade trailing edge (Fig. 2.). In [7] are presented results of the measurement of the characteristic curve of the fan, when the acrylic pipe is replaced with the aluminium duct with an array of pressure sensors.

2.2. Experimental techniques

2.2.1. Laser Doppler anemometry (LDA)

The LDA measurements were performed subsequently for all three velocities (U-axial, V-radial and W-circumferential) using the one-component LDA system along the vertical diameter at a 10-mm distance points, in both measuring sections at the test rig presented in Fig. 1. Applied LDA system is Flow Explorer Mini LDA, Dantec, with the BSA F30 signal processor. Focus is at 285 mm, laser power is 35 mW and wavelength 660 nm. It works in a backscattered mode. Transit time was used as the weighting factor. Recording time of 10 s was set up as the stop criteria for all measurements, while data frequency varied along the vertical diameter, depending of the measured velocity component. Data validation during the test was high, especially for circumferential velocity. Sensitivity was adjusted to the values 1200-1400 V. The acquisition and a part of data processing were done in the BSA software, while the major part of data processing was done by in-house codes [1,8]. Fluid flow was seeded by the Antari Z3000II fog machine using liquid EFOG, Density Fluid, Invision. Seeding was naturally sucked in the test rig by the fan.

2.2.2. Stereo particle image velocimetry (SPIV)

SPIV measurements were performed at the test rig presented at Fig. 1., in the specified measuring cross-section and vertical meridian section defined in Fig. 3. Analogue SPIV setup was in section $x/D=26.31$. The orientation of the target coordinate system is given in Fig. 3. for both planes. Here will be presented results only for the cross-section measurements, i.e. pos. 5 at the Fig. 3. Fluid flow was illuminated by the dual head Nd:Yag laser (max power: 30mJ/pulse, wavelength 532 nm, 15 Hz). Two 12-bit CCD cameras with the resolution of 1660x1200 pixels and 32 fps were in Scheimpflug setup. The INSIGHT 3G TSI software was used for data acquisition and processing, while the post-processing was performed in Tecplot and in-house programs.

Sampling rate was either 2Hz or 7 Hz. In the first case 400 pictures were taken, while in the second case, due to the RAM limitations, only 99 pictures. Image processing was performed using the central difference image correction (CDIC) deformation algorithm combined with the FFT correlator. This four-pass method employed an interrogation region of $32 \times 32 \text{ px}^2$. The vector fields are validated using

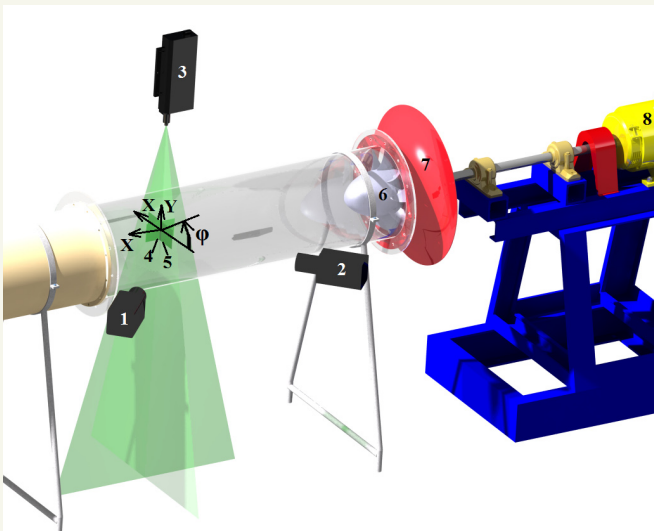


Figure 3. SPIV setup in section $x/D=3.35$: 1-left camera, 2-right camera, 3-Nd:Yag laser, 4-vertical meridian plane, 5-cross-section, 6-axial fan, 7-free bell-mouth inlet, 8-drive unit.

standard velocity range criteria and a 3×3 local median filter. Any missing vectors were interpolated using a 3×3 local mean technique. The number of interpolated vectors was, on average, around 5% [1,8]. Seeding was the same as in the case of LDA measurements.

2.2.3. High speed stereo particle image velocimetry (HSS PIV)

High speed stereo particle image velocimetry system (HSS PIV) is employed at the test rig presented in Fig. 2. HSS PIV system includes a dual oscillator-single head, diode pumped Nd:YLF laser with an output

wavelength of 532nm model Darwin Duo, Quantronix, with attached optics, adequate synchronizer and two high speed cameras Photron FASTCAM SA4, with resolution 1008x1024 at 4000 fps, and appropriate software. HSS PIV measurements have been conducted in approximately 1.4s. Cameras have been positioned in forward scatter mode. Canon EF 85mm f/1.8 USM lenses have been used. Flow was seeded by Antari Z3000II fog machine with liquid Eurolite Smoke Fluid "-X-Extrem A2". The post processing was realized by using PIVView ver. 3.3.2. Common methods of dewarping, disparity correction were applied, while the cross correlation had an interrogation area of 32x32 pixels and an overlap of 50% [7]. Fan was operating with rotation number 1200rpm.

3. Experimental results and analysis

Experiments have been performed with modern and complex measuring techniques explained below.

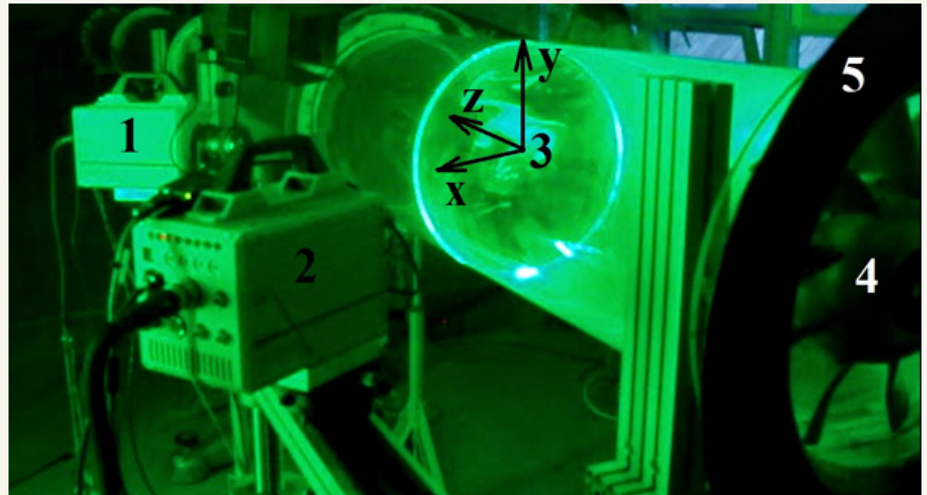


Figure 4. Measurement section for HSS PIV: 1- left, 2- right high-speed camera, 3- measuring cross-section with software convection for the coordinate sys. ($z/D=2.1$, $D=0.402\text{m}$), 4- ZP axial fan impeller and 5- profiled bell-mouth inlet.

3.1. LDA experimental results

3.1.1. Integral characteristics of turbulent flow

Radial profiles of all three velocities in both measuring sections for the fan operating regime $n=1000\text{rpm}$ are presented in Fig. 5. The angle $\varphi=90^\circ$ denotes the upper part (above-pipe axis) of the vertical diameter, while $\varphi=270^\circ$ the lower part (under-pipe axis) (Fig. 3.). Rankine vortex profile is detected in both measuring sections. Axial velocity profile doesn't change much along the pipe axis. The maximum axial velocity is almost the same in both measuring sections and reached in the sound flow region. Reverse flow is detected in both measuring sections. Circumferential velocity changes its

intensity, but not the character. It decreases from the maximum value $W_{max}=10.74\text{m/s}$, reached in the shear layer region, in the measuring section 1 to $W_{max}=6.6\text{m/s}$ in section 2 [8]. It is a decrease of almost 40%, under the influence of friction. Solid body region, with almost linear increase of the circumferential velocity, is present in the region up to the $r/R=0.2$ in the measuring section 1, while up to $r/R=0.15$ in measuring section 2 (Fig. 5.). Velocity profiles are almost symmetrical with respect to these positions. Radial velocity has finite, but not high values in the vortex core region, where its absolute max value is approx. 1m/s in the measuring section 1, while 2.09m/s in the measuring section 2.

Volume flow rate is calculated on the basis of axial velocity profile in both measuring sections and has values $Q_1=0.861\text{m}^3/\text{s}$ and $Q_2=0.837\text{m}^3/\text{s}$. Relative difference is 2.9%. Averaged axial velocity is $U_{m1}=4Q/D^2\pi=6.69\text{m/s}$, while in section 2 is $U_{m2}=6.66\text{m/s}$. Reynolds number is approximately $Re=U_m D/\nu\approx 1.9\cdot 10^5$. Average circulations, calculated on the basis of axial and circumferential velocity profiles, are $\Gamma_1=5.62\text{m}^2/\text{s}$ and $\Gamma_2=3.79\text{m}^2/\text{s}$, what proves circulation decay process downstream the fluid flow [1,2]. The important characteristic for turbomachinery, the swirl flow, is calculated as $\Omega_1=Q/(R\Gamma)=0.76$ and $\Omega_2=1.1$.

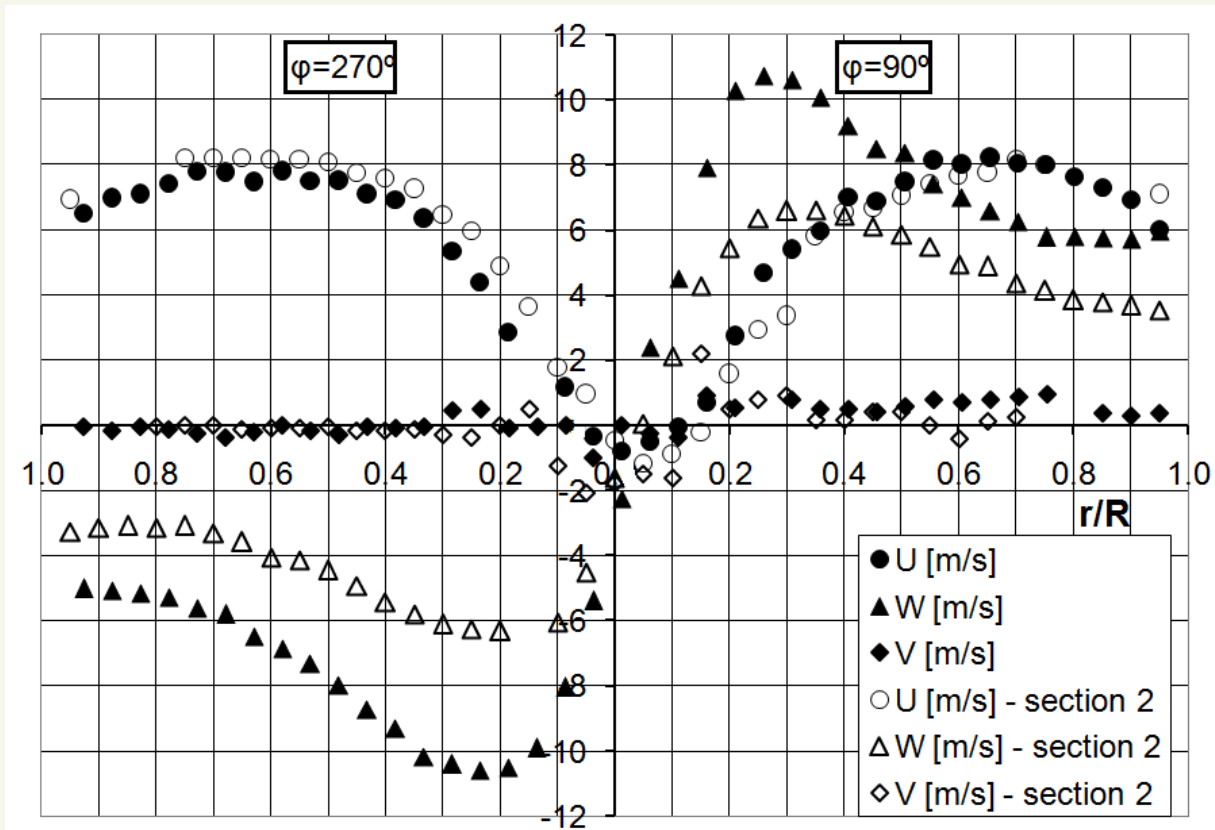


Figure 5. Distribution of time averaged velocities (U-axial, W-circumferential, V-radial) in both measuring sections.

3.1.2. Turbulence statistics

Influence of the swirl on statistical parameters and non-gradient turbulent transfer is presented in [1,3,9]. Representative statistical parameters for this fluid flow study are level of turbulence, skewness and flatness factors [1,3,4,8,9,10]. Reynolds normal stresses and turbulence intensities in defined directions are calculated as follows:

$$\overline{u_i^2} = \sum_{j=0}^{N-1} \eta_j (u_i^2)_j, \quad \eta_j = t_j / \sum_{k=0}^{N-1} t_k, \quad \sigma_i = \sqrt{\overline{u_i^2}}, \quad (1)$$

where t_j is transit time of the j -th particle crossing the measuring volume and $u_i = u, v, w$ adequate fluctuating velocities. In Fig. 6. are presented turbulence intensities in three directions (axial, radial and circumferential) for both measuring sections. The highest turbulence intensities are reached in all cases and in both measuring sections in the core region (Fig. 6.). Higher values are reached in the sound flow region for all three velocity components in the measuring section 1, while the opposite situation is in the vortex core region. Anisotropy is obvious for both measuring sections. The highest turbulence intensities are reached in both measuring sections in radial direction.

Values of the normalized central moments for all three velocity components of the third S_i order (skewness factor) and the fourth order F_i (flatness factor), are calculated in the following way:

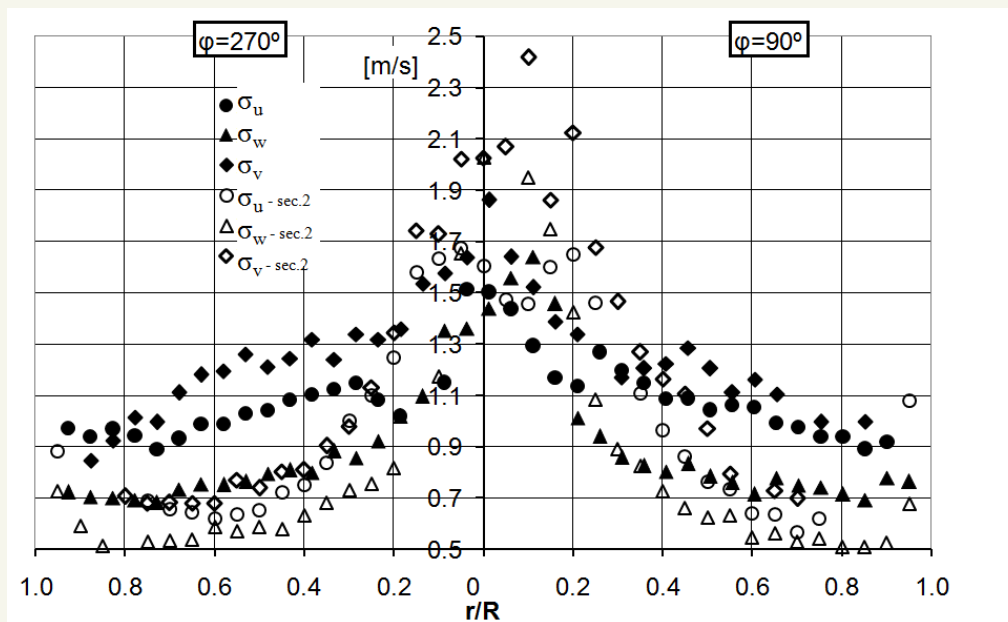


Figure 6. Distributions of turbulence intensities in three defined directions in both measuring sections.

$$S_i = \overline{u_i^3} / \sigma_i^3, \quad F_i = \overline{u_i^4} / \sigma_i^4, \quad (2)$$

where now $i = u, v$ and w . Skewness factor is indeed an asymmetry coefficient for adequate fluctuating velocity [1,3,4,8,10,11]. Radial distributions of skewness and flatness factors for circumferential fluctuating velocity in both measuring sections are presented in Fig. 7. It shows that all skewness factors differ from adequate values for Gaussian probability distribution ($S_u = S_v = S_w = 0$) and all distributions are very non-uniform. S_w changes its sign many times, what indicates various processes of turbulent diffusion, as well about complex interactions of fluctuating and deformation fields [1,8]. Normalized central moment of the fourth order represents flatness coefficient of the density of the probability distribution of fluctuating velocity [1,3,8]. High and non-uniformly distributed values of F_w correlated to the S_w in the same points reveal complex turbulent structure, as also shown in [1,3,8]. These distributions of statistical parameters reveal important relationship between average and fluctuating velocity fields.

3.1.3. Spectral analysis of the structure of turbulence swirl flow

Calculated spectral densities of the circumferential fluctuation velocity in plane $\varphi = 270^\circ$ are presented in Fig. 8.

Presented points belong to the characteristic flow regions. The largest share of energy is distributed in

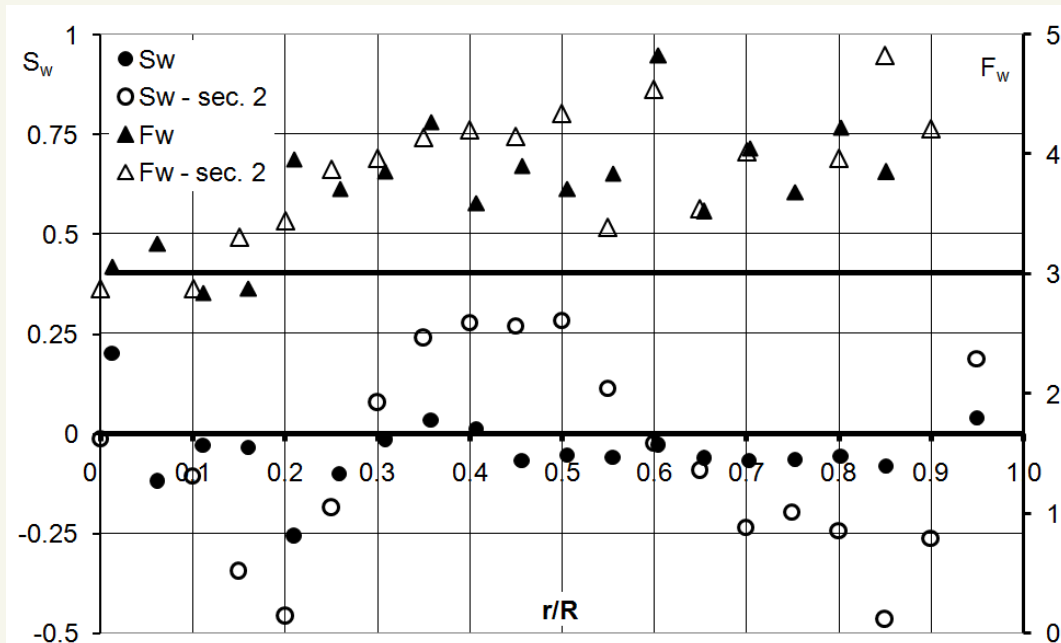
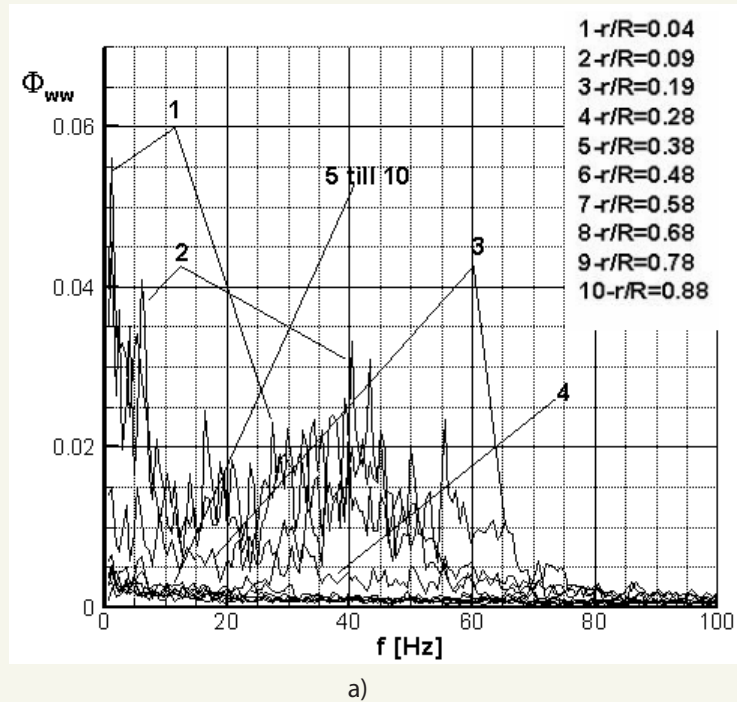
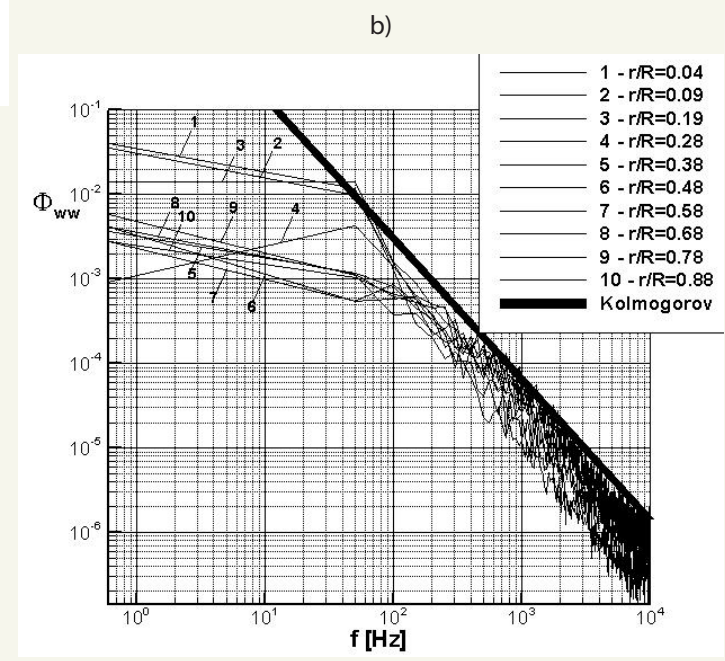


Figure 7. Skewness and flatness factors for circumferential velocity in both measuring sections (radius defined with $\varphi = 90^\circ$).

the region till 75Hz. It is obvious that the highest energy is at the pipe axis, while significantly decreases in the direction towards wall. Fig. 9.b presents spectral densities in the double log diagram after Akima spline use. High values of spectral density occur for lower frequencies, while with increase of frequency it decreases and inertial spectrum part behaves according to the Kolmogorov theory $\ddot{O}_{ww}(f) \propto f^{-5/3}$, what is



Dunaj
Dunav



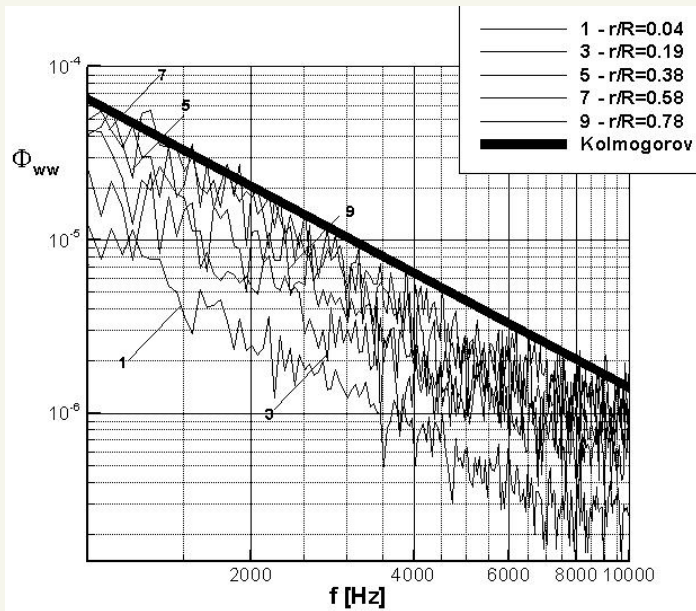
Дунай

Figure 8. Spectral densities of circumferential fluctuation velocity in section 1 in plane $\varphi=270^\circ$:
 a) till 100 Hz,
 b) double log diagram till 10kHz.

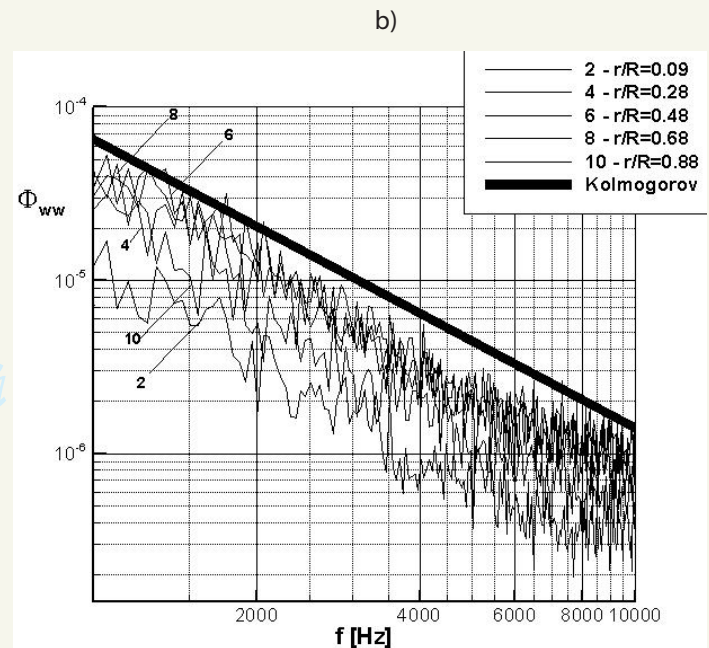
also shown in [1,4]. In Fig. 9.b are presented densities for higher frequencies. It is obvious that for higher frequencies energy is the lowest at the pipe axis and increases till the $r/R=0.58$ (Fig. 9.a), i.e. $r/R=0.48$ (Fig. 9.b). Both points are in the sound flow region. Afterwards, with r/R increase, energy decreases.

3.2. Experimental results and analysis by SPIV

SPIV measurements have been performed in a cross-section, i.e. the target plane X-Y of size 200x90 mm, where the target origin is on the pipe axis (Fig. 3.). Velocity vectors for the measuring section 1 are



a)



b)

Figure 9. Spectral densities of circumferential fluctuation velocity in section 1 in plane $\varphi=270^\circ$ for higher frequencies.

presented in Fig. 10. The maximum velocity is still not reached and measured area presents the vortex core region. It is obvious that the vortex core centre is not on the pipe axis. These results are obtained on the basis of averaging 400 pictures sampled with 2 Hz. It is shown that averaged velocity fields with 99 pictures taken with 7 Hz show the same intensity and character [1]. In paper [8] has been reported that the velocity intensity is greater in section 1 than in section 2 for the same rotation speed, i.e. Reynolds number.

Vortex core dynamics is also studied on the basis of these results. Positions of the minimum of total velocities for 400 pictures in both measuring sections is presented in Fig. 11. These minimums correspond to the vortex core center. Here the geometrical centre of all 400 positions is marked with a black cross, while the minimum of the average total velocity is marked with a grey cross. Grey cross has

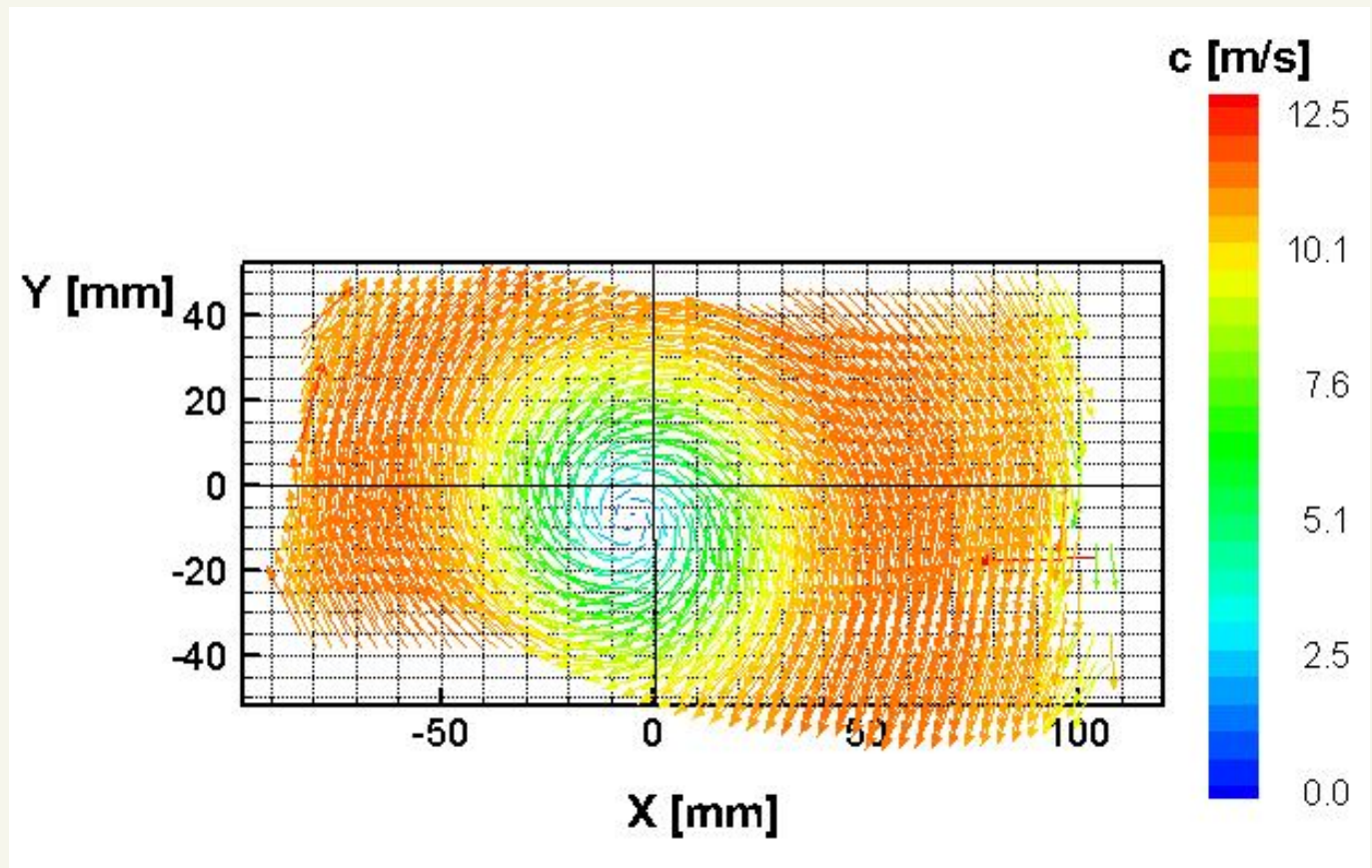


Figure 10. Velocity vectors and magnitude in cross-section in measuring section 1.

the position ($X_{\min} = -5.55\text{mm}$, $Y_{\min} = -8.08\text{mm}$) in section 1 (Fig. 11. a). It is shown that in the section 2, these two crosses overlap almost totally (Fig. 11. b). Total number of minimums (400) are not visible as some of them are repeated in one point. In measuring section 1 only 10% of the points are unique, while in section 2 this intake is higher and reaches 36%. Most of the points are multiple-repeated. It is obvious (Fig. 11.) that more narrow area of the vortex core precession movement is in the case of measuring section 1 than in section 2. All these information prove significant downstream transformation of the vortex core behaving. Similar results are obtained for higher sampling rate of 7Hz, what is shown in [1]. Various analysis techniques have been applied for the vortex core dynamics study, such as vortex core centre coordinates and correlation time dependencies, 3D histograms of the velocity minimum repetitions in measured sections and etc. [1,8].

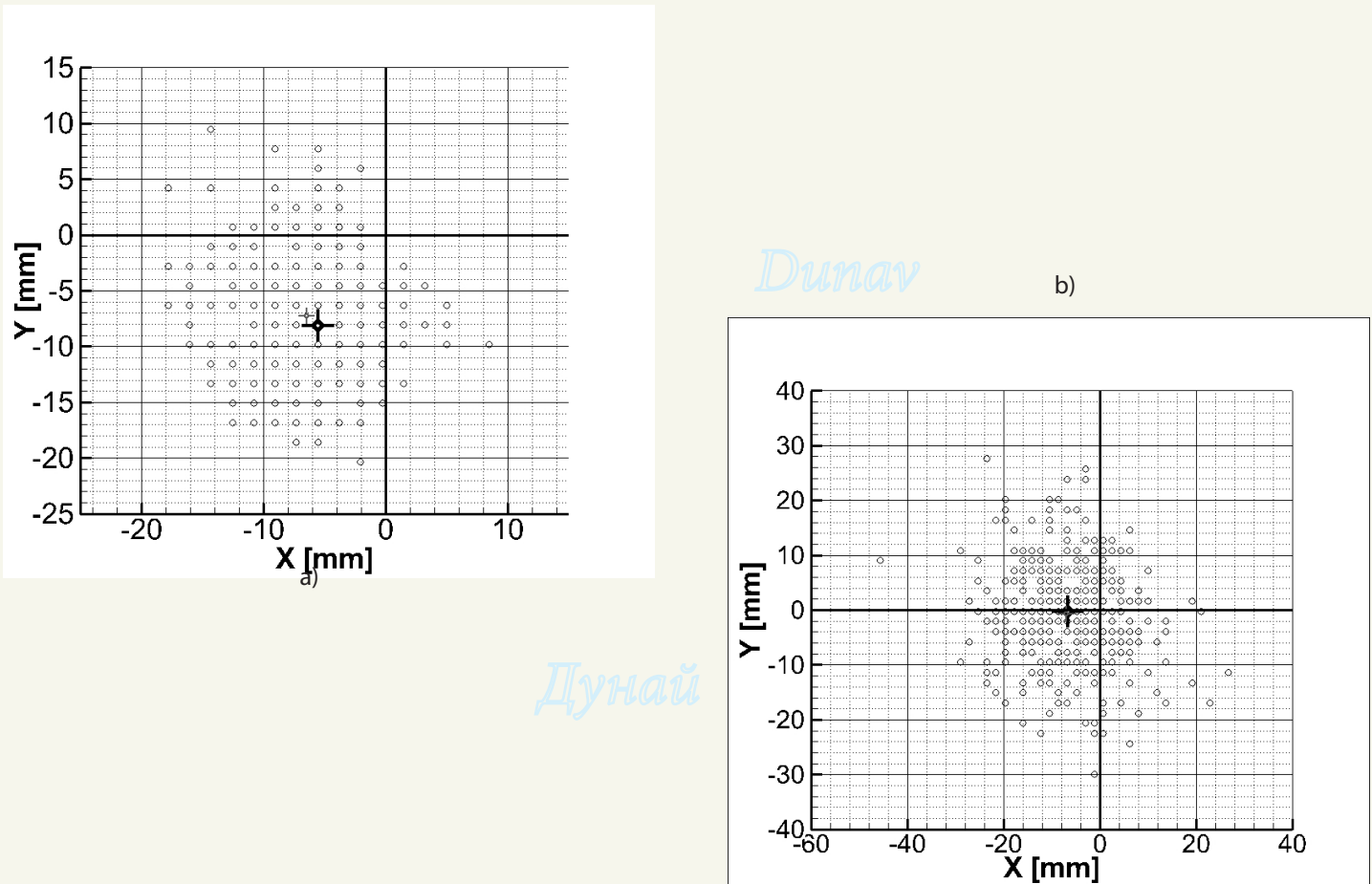


Figure 11. Positions of the total velocity minimum in both cross-sections, respectively [8].

3.3. HSS PIV measurements

The newest measuring technique High speed stereo particle image velocimetry (HSS PIV) is applied behind the axial fan, in the pipe cross-section and horizontal meridian section with center in position 2.1D from the blade trailing edge. This problem has been treated in various ways in [1,7,12,15,16]. HSS PIV measurements were performed in a cross sectional x-y plane (Fig. 12.a) and in a horizontal meridian plane z-x (Fig. 12.b), for one regime of the axial fan $n=1200\text{rpm}$.

3.3.1. Integral characteristics

On the basis of HSS PIV measurements in both x-y and z-x planes three-component velocity fields are obtained. Time-averaged velocity components (U, V and W) are afterwards calculated. These components, along radius defined with an angle $\varphi=0^\circ$, are presented in Fig. 13.a. Calculated flow

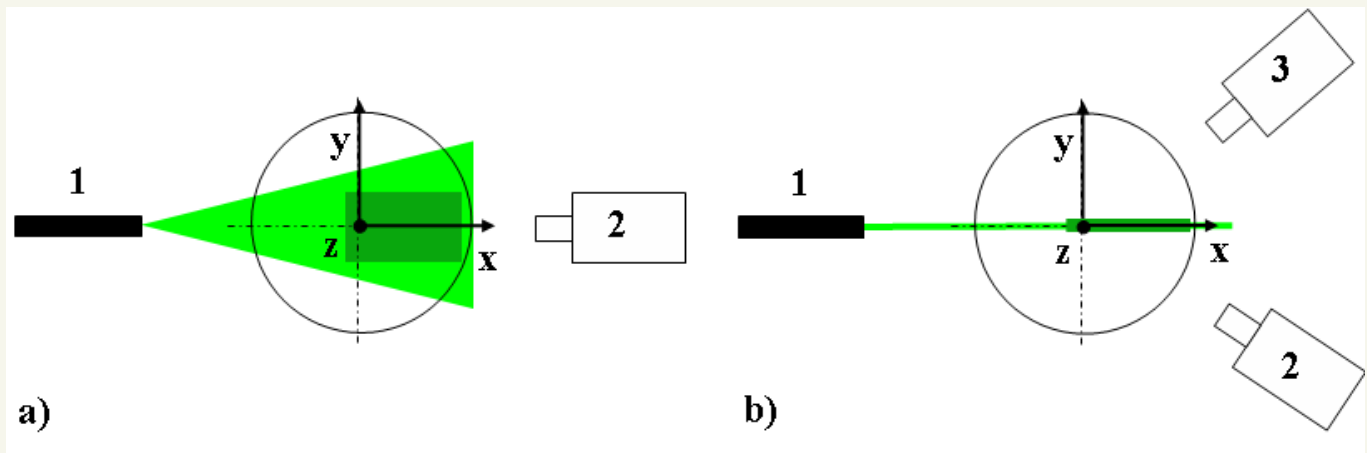


Figure 11. Positions of the total velocity minimum in both cross-sections, respectively [8].

parameters are average velocity $U_m=6.85\text{m/s}$, Reynolds number $Re=U_m D/\nu=176529$, volume flow rate $Q=0.8695\text{m}^3/\text{s}$, average circulation $\Gamma=7.98\text{m}^2/\text{s}$ and swirl number $\Omega=Q/(R\Gamma)=0.542$, where R is inner pipe radius. Radial distributions of the time averaged axial (U), radial (V) and circumferential velocities (W), for $z/D=2.1$, are presented in Fig. 13.a. Circumferential velocity distribution characterizes Rankine swirl with solid body region in the vortex core, shear layer with W_{max} , reached in position $r/R=0.325$, and wall region with almost constant circulation (Fig. 13.a) and wall region. It shows that the used swirl generator produces Rankin vortex in both cases. Axial velocity profiles, again, reveals reverse flow region. Radial velocity is approximately zero, while in the vortex core region has values $(V/U_m)_{\text{max}}=0.3$. It is interesting to emphasize that profiles of all

three dimensionless average velocities in the cross and meridian section are almost totally overlapped (Fig. 13.a). Average circulation is almost constant in the sound flow region (Fig. 13.a), what is again characteristic of this flow in the sound flow region of the Rankine vortex (free vortex region).

Total velocity field distribution in horizontal meridian section (z - x plane) is presented in Fig. 13.b. Total velocity minimum is reached in the pipe axis region, while maximum gradually reached its maximum after the shear layer region. It is almost symmetrical velocity profile with respect to the pipe axis. This indicates more centralized swirl on the contrary to the situation in the previous test rig, where the swirl center was not in the pipe axis.

3.3.2. Invariant maps

Some of experimentally obtained Reynolds stresses are presented in Fig. 14. [1,12]. Turbulence levels, again, reach maximum values for all velocities in the vortex core region (Fig. 14.a). Reynolds shear

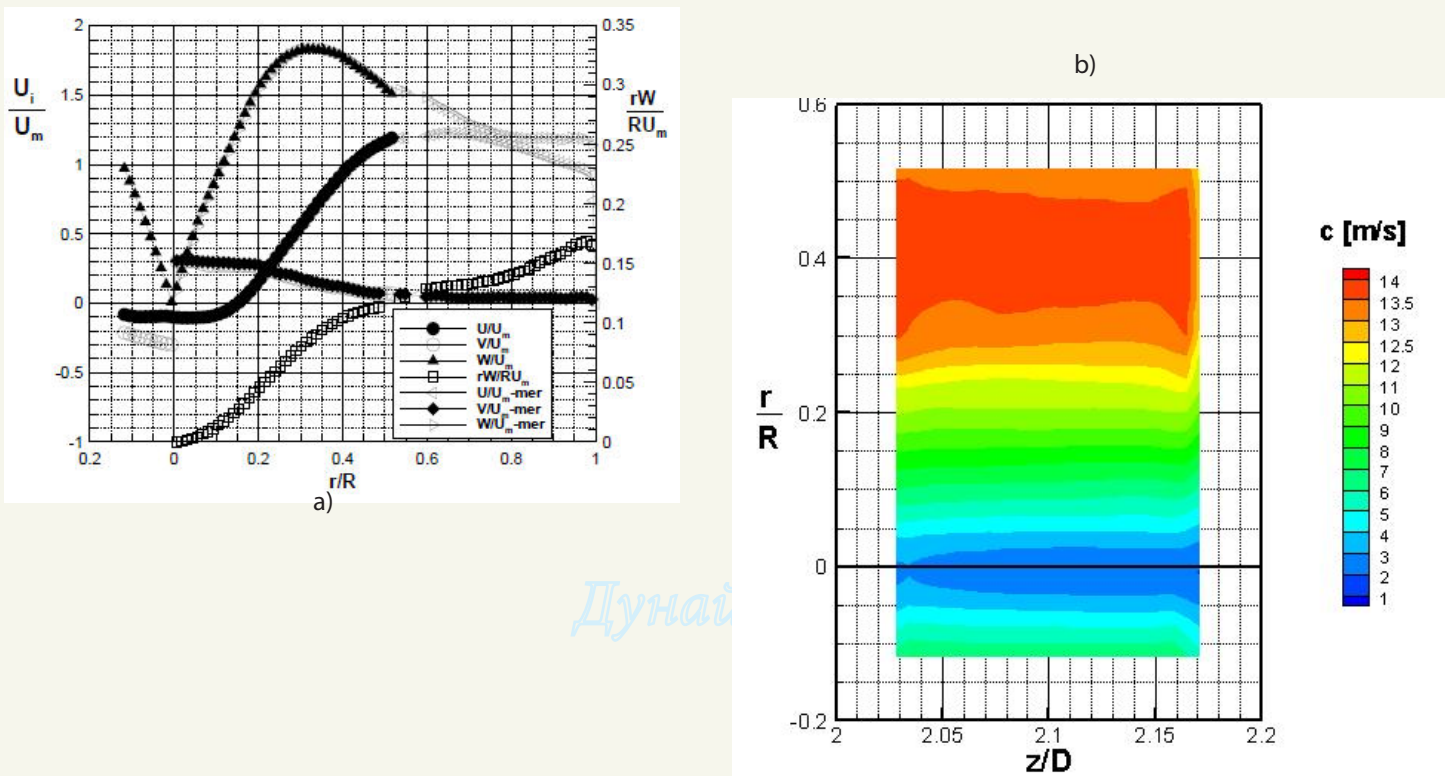
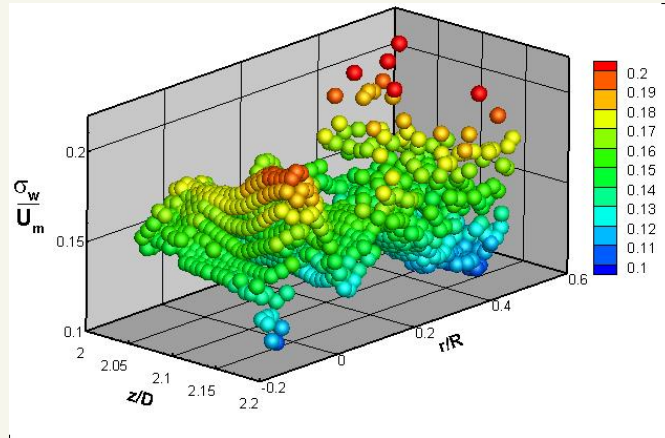


Figure 13. a) Radial distributions of time-averaged velocities and circulation ,
b) Average total velocity field in meridian section.

stresses have characteristic distribution for turbulent swirl flow.

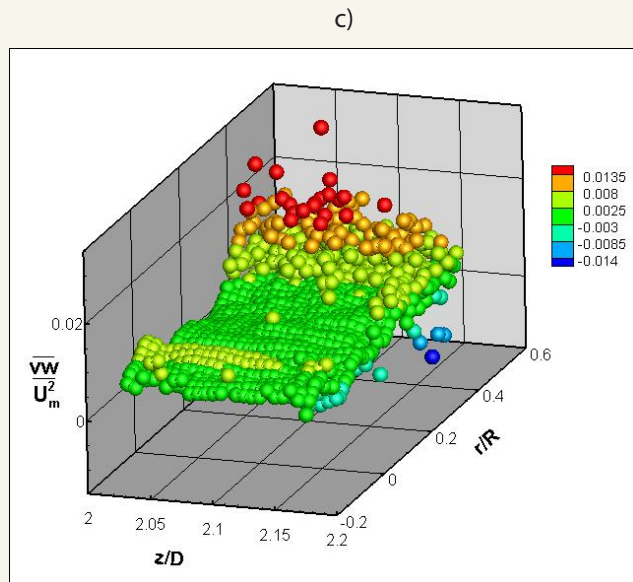
Basic idea of turbulence investigation is a quantitative description of turbulence anisotropy. Anisotropy tensor has been introduced as the measure of anisotropy, where its components are a_{ij} . Three independent invariants are expressed as:



a)

Dunaj

b)



c)

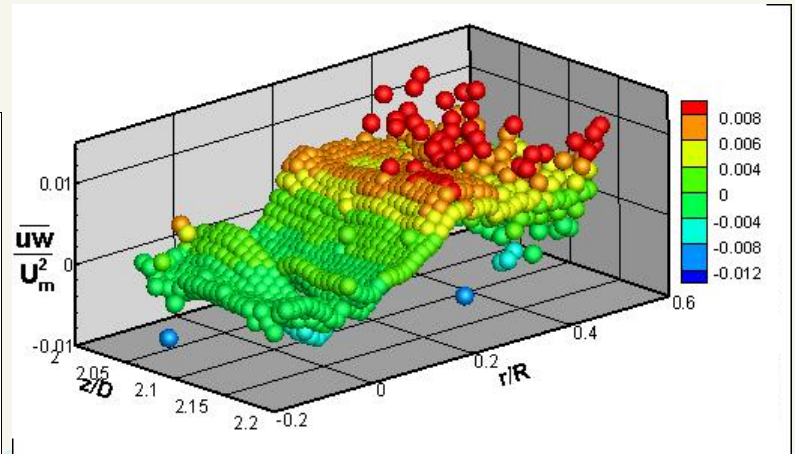


Figure 14. a) Turbulence level for circumferential velocity, b) and c) Reynolds shear stresses in meridian section.

Duna

$$I_a = 0, \quad II_a = -\frac{1}{2} a_{ij} a_{ji}, \quad III_a = \frac{1}{3} a_{ij} a_{ik} a_{jk}, \quad \text{where } a_{ij} = \frac{1}{2k} \overline{u_i u_j} - \frac{1}{3} \delta_{ij} \quad \text{and } k = \frac{1}{2} (\overline{u^2} + \overline{v^2} + \overline{w^2}), \quad (3)$$

where k is turbulence kinetic energy and δ_{ij} is Kronecker delta. Obtained invariant maps are presented in Fig. 14., of which one for the whole meridian section is in Fig. 15.a. Three-component isotropic turbulence is reached on the pipe axis (Fig. 15.b) and stays in that point for all points along pipe axis. Some measuring points, in measuring section $z/D=2.1$, reach regions of axis-symmetric turbulence contraction and expansion (Fig. 15.c).

Experimentally obtained invariant maps, by use of 2kHz HSS PIV measurements, revealed three component isotropic turbulence in the vortex core region, especially in the pipe axis zone. Experimentally determined distributions of Reynolds stresses and statistical moments give closer insight into physics of turbulent swirl flow behind the axial fan in a pipe.

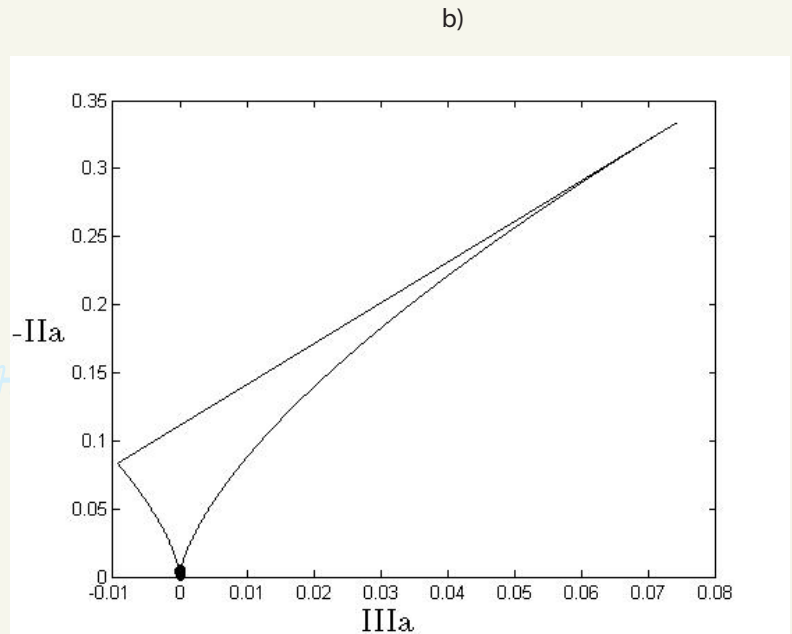
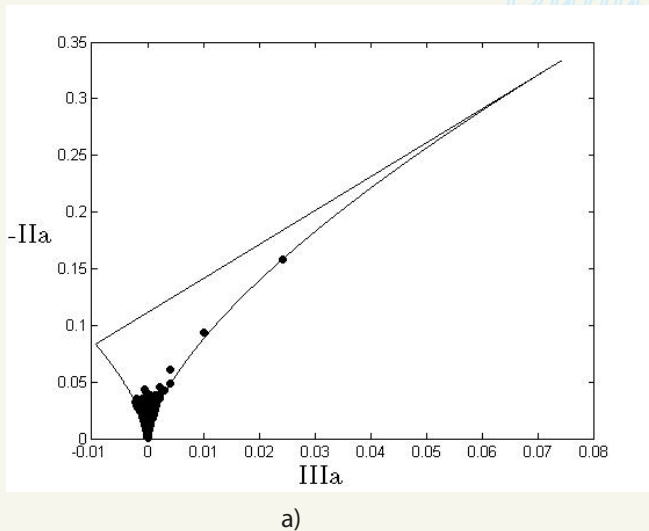
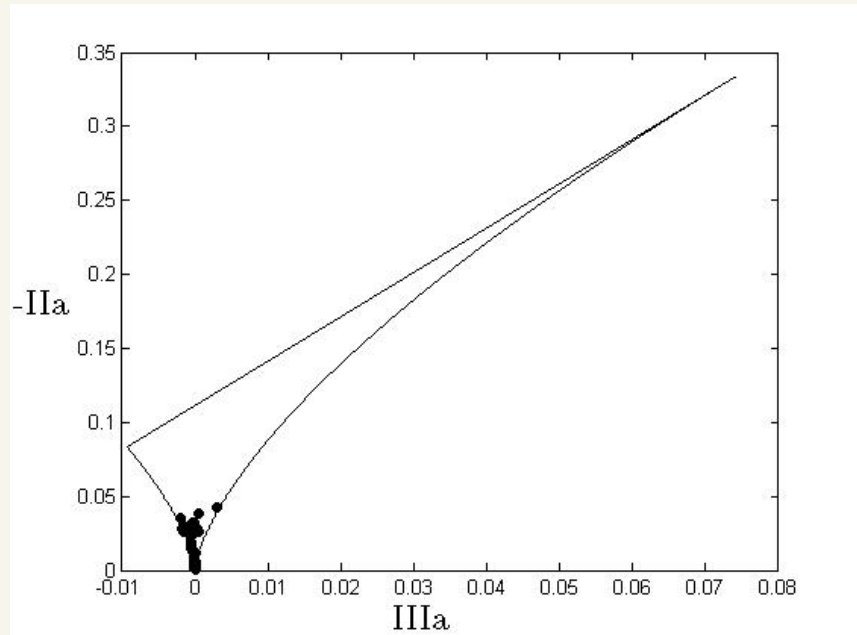


Figure 15. Invariant maps:
a) whole meridian section,
b) along pipe axis and
c) $z/D=2.1$.

Donau

Duna



c)

Dunav

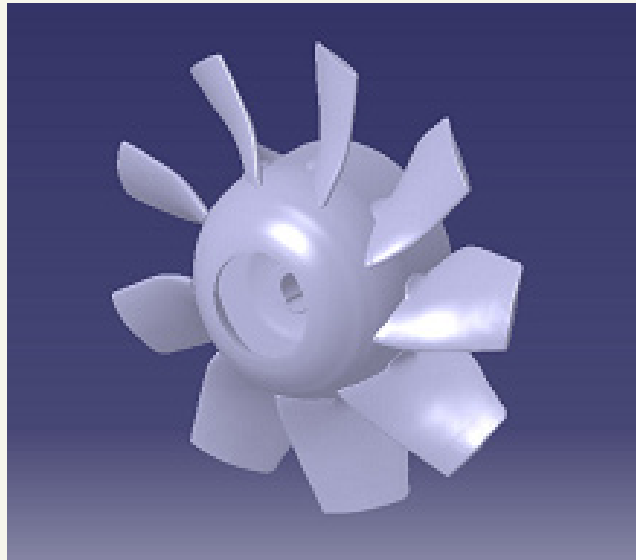
4. Conclusions

Performed LDA, SPIV and HSS PIV measurements in two various test rigs have succeeded to quantify important characteristics for the complex analysis of the turbulent swirl flow field behind axial fans. Rankine vortex structure, generated with the specially designed axial fan, is detected in both cases at the axial fan outlet. It is shown, in the case of the first test rig, that it is kept till the setup exit. Also, the intensity, especially of circumferential velocity, has been changed under the influence of the inner and wall friction. Vortex core region is smaller downstream, however not significantly. Swirl decay process is quantified by decrease of average circulation downstream. Non-axisymmetry is proved by using the LDA and SPIV measurements. Turbulence statistics proved non-homogeneity and anisotropy of the investigated flow in the case of the first test rig. Turbulence intensity has the highest values in both measuring sections in the vortex core region for all directions. All calculated values of skewness and flatness factors differ from Gaussian distribution and are very non-uniform. SPIV measurements have, also, proved non-axisymmetry and the Rankine vortex type velocities distribution. Here is also demonstrated the method for vortex core dynamics investigation with total velocity minimum location in the cross-section. Results have shown that in the downstream section, i.e. section 2, points with the repetition are more grouped around the center. It is shown that only 10% of points are unique in section 1, while 36% in section 2. HSS PIV experimental results obtained on the second test rig have, also, shown three-dimensionality and non-homogeneity of the turbulent swirl flow behind the axial fan. Good

overlapping of all average velocity profiles in meridian and pipe cross-section is obtained. Characteristic distributions of Reynolds stresses are obtained. Experimentally determined and calculated invariant maps have revealed three-component isotropic turbulence in the vortex core region, especially in the pipe axis zone. Investigations presented in this paper only, in a smaller scope, describes complexity of the treated physical problem - turbulent swirl flow. This phenomenon was the main focus of the established Bilateral Project between Karlsruhe and Belgrade Mechanical engineering faculties.

Dunaj

Duna



Дунав

Дунай

Project was financially supported by the Ministry of Education, Science and Technological Development Republic of Serbia (Bilateral Project, Head in Serbia was Prof. Dr.-Ing Svetislav Čantrak, and Project No. TR 35046) and German Academic Exchange Service (DAAD) (also Bilateral Project, Head in Germany was Prof. Dr.-Ing. Martin Gabi) what is gratefully acknowledged. Axial fan has been designed by Prof. Dr.-Ing. Zoran Protić[†] (1922-2010).

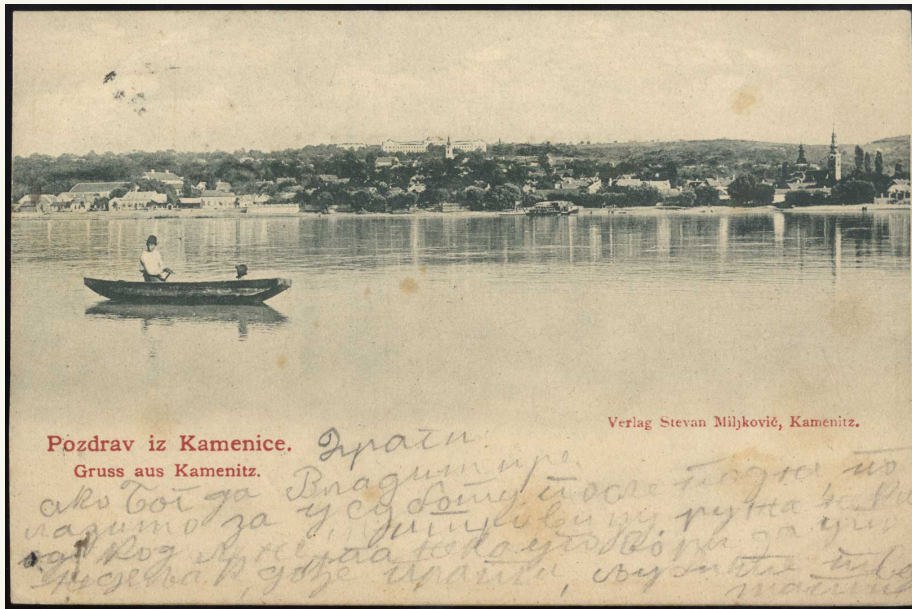
References

- [1] Čantrak Đ (2012) Analysis of the Vortex Core and Turbulence Structure behind Axial Fans in a Straight Pipe using PIV, LDA and HWA Methods, Dissertation, PhD thesis, Univ. of Belgrade, Faculty of Mech. Eng., Belgrade.
- [2] Benišek M (1979) Investigation of the Turbulent Swirling Flows in Straight Pipes, (in Serbian language), Dissertation, Univ. of Belgrade, Faculty of Mech. Eng., Belgrade.
- [3] Čantrak S (1981) Experimentelle Untersuchungen statistischer Eigenschaften turbulenter drallbehafteter Rohr- und Diffusorströmungen, Dissertation Universität Karlsruhe (TH), Institut für Strömungslehre und Strömungsmaschinen.
- [4] Lečić M (2003) Theoretical and Experimental Investigations of the Turbulent Swirling Flows, (in Serbian), Dissertation, Uni. of Belg., Fac. of Mech. Eng., Belgrade.
- [5] Ćočić A (2013) Modeling and Numerical Simulations of Swirling Flows, (in Serbian), Dissertation, University of Belgrade, Faculty of Mechanical Engineering, Belgrade.
- [6] Ilić D (2013) Swirl Flow in a Conical Diffuser, (in Serbian), Dissertation, University of Belgrade, Faculty of Mechanical Engineering, Belgrade.
- [7] Mattern P, Sieber S, Čantrak Đ, Fröhlig F, Caglar S, Gabi M (2012) Investigations on the Swirl Flow Caused by an Axial Fan: A Contribution to the Revision of ISO 5801, Fan 2012, International Conference on Fan Noise, Technology and Numerical Methods, Senlis, France, 18-20.04., CD Proc., 11 pages, fan2012-68-MATTERN.
- [8] Čantrak Đ, Nedeljković M, Janković N (2012) Turbulent Swirl Flow Characteristics and Vortex Core Dynamics behind Axial Fan in a Circular Pipe, Proceedings, Conference on Modelling Fluid Flow (CMFF'12), The 15th International Conference on Fluid Flow Technologies, Budapest, September 4-7, Vol. II, pp. 749-756.
- [9] Čantrak Đ, Gabi M, Janković N, Čantrak S (2012) Investigation of Structure and Non-gradient Turbulent Transfer in Swirling Flows, PAMM, 12, pp. 497-498.
- [10] Čantrak Đ S, Janković N Z (2013) Reynolds Number Influence on the Statistical Characteristics of Turbulent Swirl Flow, 4th International Congress of Serbian Society of Mechanics, Vrnjačka Banja, Serbia, 4-7 June, Proceedings, pp. 273-278.
- [11] Acrivelllis M, Čantrak S, Jungbluth H (1982) Statistical Properties of Turbulent Swirl Flow in Pipes, (in German language), ZAMM, Band 62.
- [12] Čantrak Dj, Mattern P, Jankovic N, Gabi M (2013) PIV Invariant Maps in Analysis of Turbulent Swirl Flow, S10.2: Turbulence and reactive flows, 84th Annual Meeting, Novi Sad, Serbia, GAMM, March 18-22, Book of Abstracts, Paper no. 67938, <http://gamm2013.cats-host.com/cms/images/documents/thematicprogram.pdf>
- [13] Protić M, Nedeljković M, Čantrak Đ, Janković N (2010) Novel Methods for Axial Fan Impeller Geometry Analysis and Experimental Investigations of the Generated Swirl Turbulent Flow, Thermal Science, Vol. 14, pp. S125-S139.
- [14] Steenbergen W, Voskamp J (1998) The Rate of Decay of Swirl in Turbulent Pipe Flow, Flow Meas. Instr., 9, pp. 67-78.
- [15] Sieber S, Mattern P, Caglar S, Gabi M (2012) Time Resolved Investigation on the Swirl Flow in the Wake of a Ducted Fan Using High Speed Stereo PIV, Fachtagung "Lasermethoden in der Strömungsmesstechnik", 4-6. September, Rostock.
- [16] Mattern P, Sieber S, Dues M, Caglar S, Gabi M (2012) Simultaneous High Speed Stereo PIV and LDA Measurements in the Highly Transient Vortical Wake of an Axial Fan, 16th Int Symp on Applications of Laser Techniques to Fluid Mechanics, 9-12 July, Lisbon.

Donau

Dunaj

Duna



унав

Dunărea